
Efficient Representation of Natural Image Patches

Cheng Guo

cheng.guo.work@gmail.com

Abstract

In the complex domain of neural information processing, discerning fundamental principles from ancillary details remains a significant challenge. While there is extensive knowledge about the anatomy and physiology of the early visual system, a comprehensive computational theory remains elusive. Can we gain insights into the underlying principles of a biological system by abstracting away from its detailed implementation and focusing on the fundamental problems that the system is designed to solve? Utilizing an abstract model based on minimal yet realistic assumptions, we show how to achieve the early visual system's two ultimate objectives: efficient information transmission and sensor probability distribution modeling. We show that optimizing for information transmission does not yield optimal probability distribution modeling. We illustrate, using a two-pixel (2D) system and image patches, that an efficient representation can be realized via non-linear population code driven by two types of biologically plausible loss functions that depend solely on output. After unsupervised learning, our abstract IPU model bears remarkable resemblances to biological systems, despite not mimicking many features of real neurons, such as spiking activity. A preliminary comparison with a contemporary deep learning model suggests that the IPU model offers a significant efficiency advantage. Our model provides novel insights into the computational theory of early visual systems as well as a potential new approach to enhance the efficiency of deep learning models.

1 Introduction

Biological neural systems are intricate masterpieces of nature's information processing mechanisms [83, 64]. Just as airplanes achieve flight without mimicking the exact structure of feathers, some intricacies of the biological neural system might arise from biological constraints than from fundamental information processing requirements [61]. Despite extensive research and significant advancements, discerning the essentials from the ancillary when constructing a computational theory for neural systems remains a challenge [40, 17, 15, 26]. Theoretical models aiming to capture detailed aspects of neural systems often rely on assumptions and approximations [38, 60, 73, 41, 104]. This may limit their applicability or neglect other important aspects.

Artificial neural networks and contemporary deep learning methodologies have been profoundly influenced by their biological counterparts [33, 48]. Yet, their primary objective is to solve specific tasks, with their merit being assessed predominantly based on their effectiveness. As a result, the question of whether these methods are principled or reflect crucial features of biological systems is often sidelined or deemed irrelevant. A notable illustration of this is the concept of efficient coding [7, 89]. Despite being a cornerstone in computational neuroscience grounded in information theory and having ample experimental support, it hasn't been a central theme in the design principles of artificial neural networks.

In this paper, we address the aforementioned problems using an *ab initio* approach. First, we identify the fundamental assumptions of an information processing system amidst the myriad features of biological systems. Next, we analyze the abstract Information Processing Unit (IPU) model solely

based on these assumptions, avoiding the emulation of commonly modeled features like spike generation activity. Lastly, we compare the results derived from our abstract IPU model with those of both biological systems and deep learning model. With this approach, we aim to provide novel insights into the computational theory of early visual systems and to aspire to enhance the efficiency of deep learning models.

We define the objectives, the means, and the characteristics of an Information Processing Unit (IPU) with the following assumptions:

Assumption A: *An IPU strives to accomplish two ultimate objectives: information transmission and input probability distribution modeling.*

To optimize survival, organisms need to accurately and efficiently relay new information throughout their systems for processing and responses. Furthermore, they benefit from predicting environmental occurrences, or in mathematical terms, understanding the probability distribution of their environment, based on both personal experiences and inherited evolutionary memory.

The first goal aligns with the efficient coding hypothesis [7, 3, 89] and has been extensively studied by the computational neuroscience community [97, 55, 2, 21, 73, 42, 24, 70].

The second goal, modeling the input probability distribution, has been explored in various contexts using different methods such as Principal Component Analysis (PCA) [31, 95], Markov Random Fields (MRF) [25], Independent Component Analysis (ICA) [9, 96], sparse coding [74], Restricted Boltzmann Machines (RBM) [36], Products of Experts (PoE) [35], Field of Experts (FoE) [81], Gaussian Mixture Model (GMM) [105], Variational Autoencoders (VAE) [43], Generative Adversarial Networks (GAN) [27], and as prior belief in Bayesian models of perception [44, 37, 90, 102].

Contrary to the abundance of studies in each of the two areas separately, only a few works have sought to investigate the relationship between the two goals [91, 37, 74]. Efficient coding leads to solutions that allocate more resources to represent input regions with high probability density. This might give the impression that optimizing information transmission would also optimize input probability modeling. What adds to the confusion is the fact that some widely-used methods, such as ICA, can be interpreted from both perspectives. Additionally, the seminal sparse coding loss function by Olshausen and Field can be derived, given certain reasonable assumptions and approximations, either from the efficient coding perspective [73] or the input probability modeling perspective [74].

In this paper, we will rigorously examine the relationships and prove that they are two distinct optimization problems. As a result, there's no guarantee that the optimal solution for one goal will also be optimal for the other. We will also compare different pragmatic strategies to achieve these two goals.

Assumption B: *Both the input and output of the IPU are discretized, with the number of output states N being significantly fewer than the number of input states M ($N \ll M$).*

On the output end, neurons produce either spikes or graded outputs. Spikes are discrete events. Rate coding, therefore, offers limited resolution within a predetermined time frame. In temporal coding, the timing of spikes also has finite resolution [5, 14]. For graded outputs, biological constraints limit the resolution. For instance, luminance resolution levels at synapse terminals in a zebrafish's retina are just around 10 [71].

On the input end, those neurons receiving inputs from other neurons, consequently possess finite input states. For sensory neurons, external signals undergo conversion into biochemical signals, which due to molecular constraints, have finite resolution. Moreover for visual signals, the quantization of light into photons by quantum mechanics also establishes an ultimate constraint on resolution.

When neurons receive inputs from others, it is evident that $N \ll M$ given that $M \sim N^L$, where L is the number of inputs. For sensory neurons, as illustrated in the zebrafish example, the relationship $N \ll M$ holds true. Even if, for some sensory neurons in certain species, the relationship $N \ll M$ is not evident, we can still group both the sensory neurons and the neurons receiving their outputs into a single IPU model, ensuring $N \ll M$ holds. With $N \ll M$, information passing through each IPU undergoes significant compression post-processing, setting the stage for subsequent processing tasks.

Assumption C: *In the limit $M \rightarrow \infty$, the input is continuous, and in the limit $N \rightarrow \infty$ the IPU transformation is a smooth function.*

This assumption has been explicitly or implicitly used by all previous studies that rely on methods such as series expansion, calculus, and differential equations [97, 2, 24]. Without continuity, a model cannot infer based on the knowledge of the immediate neighbors of data points, and it cannot learn.

Assumption D: *The IPU transformation is deterministic.*

For simplicity in this study, we examine only the noiseless case where the IPU transformation is deterministic. We argue that this is a good approximation because responses of neurons in the early visual system to repeated stimuli have been found to be highly reproducible [58, 10].

Based on these assumptions, this exploration is undertaken incrementally, starting from a single pixel and progressively advancing to image patches. We propose two types of loss functions to ensure the outputs of the IPU are as independent as possible, either by explicitly enforcing output statistics, as in the case for two-pixel (2D) systems, or by achieving this implicitly by making the response vectors repel each other, as in the image patches cases.

2 One Pixel

We begin with the simplest conceivable case, where the input to the model consists of a single pixel with one color channel. Although seemingly trivial, this model can represent various biological units. For example, it could model the eyespot of single-celled organisms like Euglena, the large monopolar cells found in an insect’s compound eye or the bipolar cells in the retina. The single pixel case has been studied by many authors [46, 2, 24]. We aim to revisit it to introduce the concepts and notation.

Let us denote the light intensity of the pixel as x , and let $p(x)$ represent its probability distribution. As the first stage in an organism’s information processing system, the single pixel IPU carries the same dual objectives as later stages: to transmit information about x efficiently through its output and to learn $p(x)$. Information is quantified by Shannon’s entropy:

$$H_p = - \sum_{i=1}^M p(x_i) \log p(x_i). \quad (1)$$

Under Assumptions B and D, the IPU employs the many-to-one step function $y = f(x)$ to map the input x into N distinct groups in the output space. Each of these groups corresponds to a fixed value of y . We denote all x values in group j as G_j , and the size of this group as n_j . The entropy of the output is given by

$$H_Q = - \sum_{j=1}^N Q(y_j) \log Q(y_j), \quad (2)$$

where $Q(y_j)$ represents the probability distribution of the output states. In this paper, we use a capital letter to denote the distribution over the output states, and a lowercase letter for the distribution over the input states.

To optimize the goal of information transmission, we need to maximize the rate of transmission, or the mutual information between input and output [7, 55]. Many previous studies model a neuron’s spike activity as a probabilistic event, which makes the mapping from stimuli to responses probabilistic. In this case mutual information is difficult to compute and they often have to resort to approximations [79, 42, 24]. However, our abstract IPU model is deterministic (Assumption D), and the mutual information simply equals H_Q (see proof in Appendix A). Maximizing H_Q is much easier to deal with both analytically and numerically.

Simultaneously, an IPU should also strive to fulfill the second objective: to model $p(x)$. Mathematically, this involves minimizing the Kullback–Leibler divergence (KL-divergence) between $p(x)$ and the distribution learned by the IPU $q(x)$. Next, we investigate the relationship between the two goals using our IPU model and determine whether an optimal solution for one leads to the optimal solution for the other.

3 Relation Between the Two Goals

To determine how an IPU models $p(x)$ we need to translate the output probability distribution $Q(y)$ into the input space as $q(x)$. $q(x)$ is a step function:

$$q(x) = q_j, \text{ for } x \in G_j, \quad (3)$$

and we have the following relations:

$$Q(y_j) = \sum_{x \in G_j} p(x) = \sum_{x \in G_j} q(x) = n_j q_j. \quad (4)$$

Minimizing the difference between $p(x)$ and $q(x)$ can be achieved by minimizing their Kullback–Leibler divergence:

$$D_{KL}(p||q) = H_{pq} - H_p, \quad (5)$$

where H_{pq} is the cross entropy. It can be proved that the cross entropy H_{pq} is equal to the entropy of the learned distribution in the input space defined as (see proof in Appendix B):

$$H_q = - \sum_x q(x) \log q(x), \quad (6)$$

and we get

$$D_{KL}(p||q) = H_q - H_p. \quad (7)$$

Since H_p is fixed, minimizing the KL-divergence requires minimizing H_q . The previous question now transforms into understanding the relationship between maximizing the entropy of the distribution in the output space (H_Q) and minimizing the entropy of the learned distribution in the input space (H_q).

Suppose we have two adjacent zones in the transformed space where the corresponding $Q(y_1)$ and $Q(y_2)$ are not equal; let's assume $Q(y_1) > Q(y_2)$. One can reduce the inequality by shifting the boundary between these two zones and moving one x value from G_1 to G_2 . Due to Assumption B, this shift corresponds to a small change in probability, denoted as δ , for both zones. Furthermore, under Assumption C, the value of δ is comparable to q_1 and q_2 . We know that reducing the inequality of $Q(y_1)$ and $Q(y_2)$ always increases H_Q . If the two optimization problems are the same, then H_q should increase; if they are contradictory, H_q should decrease. The change of H_q can be calculated as:

$$\begin{aligned} \Delta H_q &= -[Q(y_1) - \delta] \log \frac{Q(y_1) - \delta}{n_1 - 1} - [Q(y_2) + \delta] \log \frac{Q(y_2) + \delta}{n_2 + 1} \\ &\quad + Q(y_1) \log \frac{Q(y_1)}{n_1} + Q(y_2) \log \frac{Q(y_2)}{n_2} \end{aligned} \quad (8)$$

$$= q_2 - q_1 + \delta \left(\log q_1 - \log q_2 + \frac{1}{n_1} + \frac{1}{n_2} \right) + O(\delta^2) + O\left(\frac{1}{n_1^2}\right) + O\left(\frac{1}{n_2^2}\right) \quad (9)$$

$$\approx q_2 - q_1 + \delta \log \frac{q_1}{q_2}. \quad (10)$$

We can see ΔH_q can either be positive or negative, depending on q_1 and q_2 . Therefore, we have proven that optimize information transmission and optimize input probability distribution modeling are not identical, and there is no guarantee that optimum can be achieved for both simultaneously. The above derivations also applies to multivariate scenarios, as no assumptions about one-dimensionality of the input were made.

A pragmatical method to achieve the two goals is to find a suitable compromise. This approach aligns with the sparse coding method [73]. Minimizing the mean squared reconstruction error used in sparse coding is a reasonable first approximation of maximizing the mutual information between inputs and outputs [98, 6]. It also approximates the minimization of the KL-divergence between the actual and modeled probability distributions [74].

The primary limitation of this approach is that neither of the two optimization goals is achieved optimally. For early-stage IPUs, we argue that optimizing information transfer is more pressing and critical than accurately learning the input probability distribution. Early-stage IPUs should prioritize maximizing H_Q to produce a uniform output probability distribution, thereby retaining maximum

information from the input. If a more refined modeling of $p(x)$ is necessary, we can increase the output resolution N of the IPU. We will refer to this approach as even coding.

Before delving into subsequent sections where we apply even coding to more complex inputs, we wish to elaborate further on how the IPU models $p(x)$. In the IPU transformation, represented by $y = f(x)$, the output is y , not a probability. So, how can it model the probability distribution $p(x)$ and convey this information to subsequent stages? The answer lies in the nature of $y = f(x)$. It's not an arbitrary function but a deterministic step function that uniformly partitions the input probability distribution. Each value of y corresponds to an equal segment of $p(x)$. From Eq. (3) and Eq. (4) (or the relation $q(x) = \sum_y p(x|y)Q(y)$) we get

$$q(x) = \frac{Q(y_j)}{n_j} = \frac{1}{N} \frac{1}{n_j}. \quad (11)$$

Since n_j denotes the size of the group to which x belongs, it is a step function of x . Thus, $q(x)$ is the step function that the IPU uses to approximate $p(x)$. The IPU's approach to approximating $p(x)$ stands in contrast to many probability modeling methods that explicitly use optimization objectives such as KL-divergence. This also offers a potential perspective to address the foundational question of how priors, commonly employed in Bayesian models of perception, are represented in the brain [57, 93, 24].

4 Two Pixels

For two pixels, (x_1, x_2) or \mathbf{x} , we can either use a single IPU directly to model $p(\mathbf{x})$ or employ two IPUs to mode $p(x_1)$ and $p(x_2)$ separately, followed by another IPU to model the outputs $p(y_1, y_2)$. We will use the second approach, as processing as much information locally reduces the cost of information transfer. In fact, when images are stored on computers, gamma encoding is utilized to create an approximately even distribution of pixel values. When these images are displayed, pixel values undergo gamma correction to recover the original statistics for human eyes to process. In the following sections, we will assume that all pixel values x have already been processed by dedicated IPUs, resulting in a roughly even probability distribution.

The probability distribution $p(x_1, x_2)$ of natural images is relatively simple. The majority of the probability is concentrated around the diagonal line $x_1 - x_2 = 0$, with $p(x_1, x_2)$ rapidly decaying as $|x_1 - x_2|$ increases ((refer to Fig. 1 (a) as an example). Intuitively, we can use lines parallel or/and perpendicular to $x_1 - x_2 = 0$ to divide the probability distribution into even partitions.

4.1 One Basis

To investigate how IPUs learn $p(\mathbf{x})$, we conduct numerical experiments using a multilayer perceptron (MLP) as the IPU to approximate $y = f(\mathbf{x})$ and model $p(\mathbf{x})$ [68]. Other function approximation methods may also be applicable. To partition the input probability distribution using a single set of parallel lines, only one IPU with N output nodes is needed to represent N independent states. According to even coding, for each input, only one of the N output nodes should be activated, and the probability of activating any one of the N output nodes should be equal. We use the softmax function as the last layer of the MLP to ensure each output value is within $[0, 1]$, and that if a node is activated (output value equals 1), it is the only node being activated. We use stochastic gradient descent and the following loss function to train the IPU with N independent states (IS):

$$E_{IS} = \sum_i \langle y_{si} \rangle_s \log \langle y_{si} \rangle_s + k \left\langle - \sum_i y_{si} \log y_{si} \right\rangle_s. \quad (12)$$

y_{si} represents the value of the i -th output node for the s -th input sample, while $\langle \cdot \rangle_s$ denotes the average over all samples in a training batch. The first term in the loss function ensures each output node has an equal chance to be activated on average. The second term promotes activation of only one node per input sample while suppressing the remaining nodes, mimicking lateral inhibition when combined with the softmax function. The factor k balances the two terms to achieve the desired result. Fig. 1 (a) show the results learned by MLPs with 16 output nodes. To demonstrate the flexibility of the method we generated an artificial two pixel intensity probability distribution which is a 2D normal distribution. Fig. 1 (b) shows the results learned by a MLP with 200 output nodes. The size of the hexagonal lattice gradually increase from the center to the periphery to account the decrease of probability density so that each cell roughly contains same portion of probability.

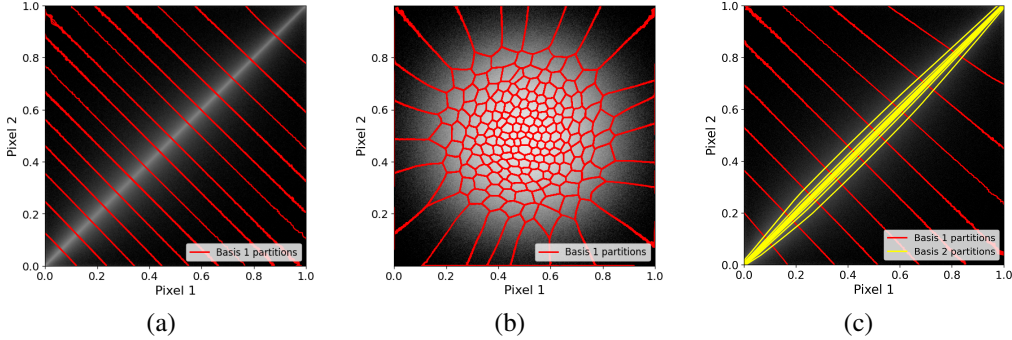


Figure 1: Evenly partitioning the two-pixel probability distribution learned by multilayer perceptrons (MLPs). The X and Y axes represent the intensities x_1 and x_2 of the two pixels. The quantity $n(x_1, x_2) + 1$ is plotted in gray on a log scale, where $n(x_1, x_2)$ denotes the number of occurrences of the two-pixel values among the sampled data. Color lines indicate the boundaries of states for each basis learned by an MLP, with one color representing one basis. (a) One basis with 16 independent states, which partitions the two pixel intensity space based on the total intensity $x_1 + x_2$. (b) One basis with 200 independent states partitions an artificial two pixel intensity which is a 2D normal distribution with a learned hexagonal lattice. (c) Two orthogonal bases, each with 10 independent states, dividing the two pixel intensity space based on the total intensity $x_1 + x_2$ and the contrast $x_1 - x_2$ approximately.

4.2 Multiple Bases

To partition the input space with two sets of orthogonal lines we need two MLPs. The orthogonality is achieved by enforcing

$$Q(y_1, y_2) = \frac{1}{N_1 N_2}, \quad (13)$$

where N_1 and N_2 represent the number of output nodes of the two MLPs (refer to Appendix C for proof). If more than two orthogonal bases are required for partitioning the space, we can enforce Eq. (13) for each combination of two bases to ensure orthogonality between them. The loss function for multiple orthogonal bases with independent states (OBIS) is

$$E_{\text{OBIS}} = \frac{1}{\binom{B}{2}} \sum_{\langle b, b' \rangle} \sum_{ij} \langle y_{bsi} y_{b'sj} \rangle_s \log \langle y_{bsi} y_{b'sj} \rangle_s + \frac{k}{B} \left\langle - \sum_{b=1}^B \sum_i y_{bsi} \log y_{bsi} \right\rangle_s, \quad (14)$$

where b is the basis index, and B is the number of bases. $\sum_{\langle b, b' \rangle}$ denotes the sum over all $\binom{B}{2}$ combinations of two distinct bases. y_{bsi} represents the value of the i -th state in base b for the s -th input sample. The first term ensure all $N_1 N_2$ combinations of (y_1, y_2) are equally likely, satisfying Eq. (13). The OBIS loss function Eq. (14) is a generalization of Eq. (12).

Fig. 1 (c) shows an example of two-pixel input space partitioning using two orthogonal bases. For a more detailed discussion on the experiments and additional results, refer to Appendix D.

Even though we introduce the loss functions Eq. (12 and Eq. (14 with two pixel system as example, They can be used beyond 2D and even to high dimensional case such as small image patches. Additionally, it's worth noting that OBIS might model grid cells [29] in the entorhinal cortex, though this topic is beyond the scope of the current paper.

5 Image Patches

Next, we move on to study image patches. The multivariate input probability distribution $p(\mathbf{x})$ is considerably more complex compared to the previous examples. In principle, the loss functions formulated in the previous section can be adapted for image patches. While our preliminary results are promising, certain issues arise.

First, if we use only one basis to discretize $p(\mathbf{x})$ (e.g. Fig. 1 (b)), the required number of states for a good approximation would be very large, making the evaluation of the softmax function computationally expensive. On the other hand, using multiple orthogonal bases would also significantly increase the computational cost to ensure orthogonality if the number of bases is more than just a few. Additionally, determining the optimal number of bases and the number of independent states for each basis is an open question.

Second, we want the representation to capture the similarity between image patches. However, using OBIS makes it difficult to gauge input similarity through methods such as calculating the difference between representations. For OBIS, all states are considered equal and lack an inherent order. Even if we could establish an order for the states within each basis, we would still need to define a method for comparing values across different bases.

As a result, a more efficient and apt coding scheme is needed for handling the complexities of inputs like image patches. Unlike OBIS, real-valued vectors in \mathbb{R}^N have well-defined metrics and have been successfully used to represent a diverse range of entities, including images, texts, sound, proteins and categorical variables [34, 66, 1, 84, 28]. Nevertheless, if we want the representation \mathbf{y} to reflect input similarity, each value of \mathbf{y} should encapsulate all samples perceived as identical within the same group G . Under this constraint, $Q(\mathbf{y})$ cannot remain exactly constant everywhere, thereby conflicting with even coding in its strictest sense. However, a more relaxed application of the principle could still approximately hold. We can permit the representation to reflect input similarity at the most granular level, while enforcing even coding at a larger scale in the transformed space. We will detail this method in subsequent sections.

5.1 Loss Function

Inspired by the principles of contrastive learning and related methods [13, 85, 45, 16], we introduce a loss function that makes input samples repel each other in the transformed space to promote even distribution. The repulsive force diminishes with increasing distance, as described by the following equation:

$$E_{\text{RF}} = \langle -\log \|\mathbf{y}_s - \mathbf{y}_{s'}\|_1 \rangle_{\langle s, s' \rangle}. \quad (15)$$

In this equation, $\|\cdot\|_1$ denotes the ℓ^1 norm, and $\|\mathbf{y}_s - \mathbf{y}_{s'}\|_1$ is the Manhattan distance between the representations of samples s and s' . The term $-\log \|\mathbf{y}_s - \mathbf{y}_{s'}\|_1$ represents the potential energy due to the repulsive force, which is inversely proportional to the Manhattan distance. Alternative forms of potential energy and distance measures could also be applicable. The notation $\langle \cdot \rangle_{\langle s, s' \rangle}$ denotes the average taken over all unique pairs of samples.

Should numerous samples converge at one point in the transformed space, they will exert a strong repulsive force in the surrounding area, thereby discouraging other samples from occupying nearby positions. To prevent samples from pushing each other infinitely far apart, we restrict the representation values to be within the range $[0, 1]$. With this constraint, the repulsive force pushes samples towards the vertices of the unit hypercube, effectively reducing the representations from real vectors to binary vectors as shown in Fig. 2 (a). As a result, an even distribution is achieved on a larger scale in the transformed space, which consists solely of the vertices.

For binary vectors, the collection of output nodes can be viewed as a vocabulary, and the nodes activated by an input image patch serve as its representative tokens. Unlike fixed-length representations with real-valued vectors, binary representations can employ fewer tokens for more common image patches (e.g., homogeneous patches), and more tokens for less common, structurally-rich patches. This could be advantageous if there are certain asymmetrical properties between the binary states, such as requiring more energy to be in the activated state. In this case, we add a second term to introduce asymmetry to the loss function, which echoes the sparsity regularization term found in various studies [21, 49, 72, 75, 79, 11]. The updated loss function becomes:

$$E_{\text{RF}} = \langle -\log \|\mathbf{y}_s - \mathbf{y}_{s'}\|_1 \rangle_{\langle s, s' \rangle} + \alpha \langle \|\mathbf{y}_s\|_1 \rangle_s, \quad (16)$$

where α is a free parameter to adjust asymmetry or sparsity.

In practice, we add a small value $\epsilon = 10^{-38}$ to the distance, allowing slightly different samples to share the same representation and enhancing numerical stability. Another approach to improve numerical stability involves using a theoretically equivalent form of the loss functions [69]. Instead of making samples repel each other in the output space, this approach makes nodes repel one another, encouraging output nodes to be as independent as possible.

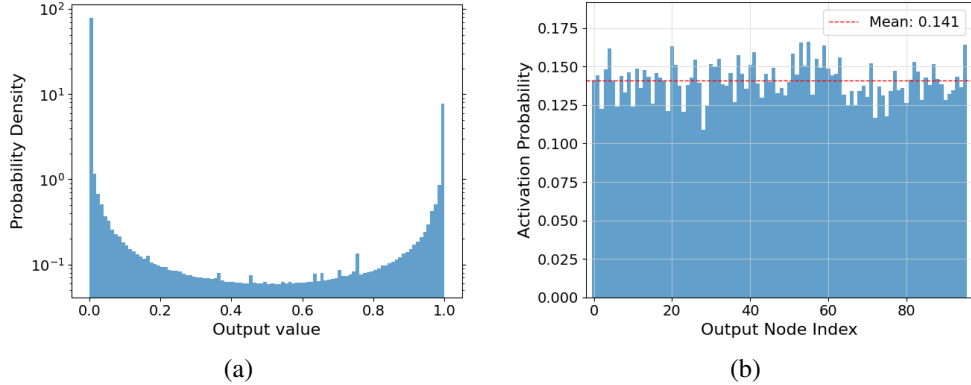


Figure 2: Statistical analysis of the learned representation using the loss function Eq. (16). (a) Histogram of the model’s output values on a log scale. Vast majority of the output values are either at 0 or 1, signifying that our model encoded the images using binary representation. (b) Probability of an output node being activated by a random image patch.

5.2 Experiments

In the following experiments, we either use a single MLP with N outputs or N MLPs, each with one output, as the IPU to approximate the transformation function $\mathbf{y} = f(\mathbf{x})$ and model $p(\mathbf{x})$.

The last layer of the MLP is a sigmoid layer, ensuring the output value ranges between 0 and 1. Our training data consist of random image patches extracted from the COCO 2017 image dataset [54] or the ImageNet dataset [18]. Unlike ICA or sparse coding, we do not use any image preprocessing. Additional training details are provided in Appendix E.

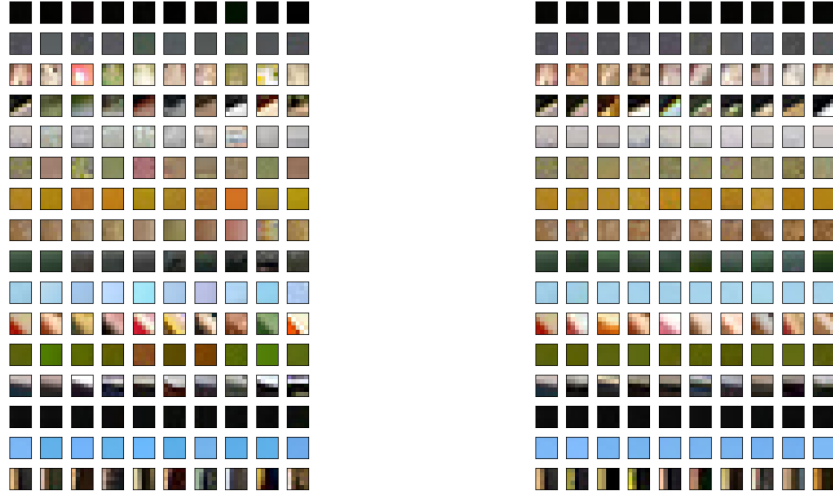
5.2.1 Output Statistics

First, we analyze the statistics of the learned representation. Across all experiments, we observe qualitatively similar output statistics, irrespective of the IPU architectures and training specifics, provided the training has properly converged. For illustration, we present an example using an IPU model trained on 5×5 color image patches. It uses 96 MLPs, each with one output node and a middle layer of 48 nodes. Following training, the model is used to generate representations for 1 million random image patches for this analysis.

Fig. 2 (a) presents the histogram of output values on a logarithmic scale. Though the outputs can be any real value between 0 and 1, after the model has been trained vast majority of the output values are either at 0 or 1, signifying that our model encoded the images using binary representation. As such, during inference, we can round the outputs to yield a true binary representation. Fig. 2 (b) illustrates the probability of an output node being activated by a random image patch. All nodes demonstrate similar activation probabilities, indicating an even distribution at this coarse scale. Further statistical analysis of the output representation is in Appendix F confirms that even distribution is also achieved at smaller scales. Therefore, the nonlinear even coding IPU can achieve statistically independent responses in a single step, eliminating the need for preprocessing steps like whitening or postprocessing steps such as divisive normalization [86].

5.2.2 Image Patch Similarity

Next, to examine how the learned representation reflects the similarities between image patches, we analyze image similarity in Fig. 3. To create this visualization, we use the following steps: We randomly sample 1 million 5×5 color image patches from the datasets. For each image patch, we use the same 5×5 color image patch model as before to generate a representation, which is a binary vector of size 96 (12 bytes). For comparison with deep learning methods, we also use the first 10 layers of a convolutional neural network (VGG16) [92] pre-trained on ImageNet to generate another representation for each image patch, which is a floating-point vector of size 128 (512 bytes). Out of the 1 million, we selected 16 random image patches and plotted them as the first column in Fig. 3 (a) and (b). For each of the 16 random images, we calculated the distance to the remaining images



(a) Even coding model with 96 binary outputs (b) Deep learning model with 128 float outputs

Figure 3: Image patches with the shortest distance in the representation space to 16 randomly selected image patches. The first column displays the 16 random image patches, while the succeeding nine columns display patches that are closest to the first-column patches in the same row. (a) Distances are computed using an even coding IPU model with 96 binary number outputs. (b) Distances are computed using the first 10 layers of a pretrained convolutional neural network model (VGG16) with 128 floating-point number outputs.

using the representations generated before, and we chose the top 9 image patches with the smallest distances and showed them in the remaining 9 columns in Fig. 3 (a) and (b) in order, respectively.

We can see in Fig. 3 (a) the learned representation clearly captures perceptual similarity. The results shown in Fig. 2, Fig. 3 (a), and additional results in Appendix F confirm that, with the loss function Eq. (16), we can indeed learn a representation which reflects the image similarity while adhering to even coding. Also, our IPU model produces comparable results to those generated with the deep learning model while using less than 3% of the memory. This illustrates the efficiency of our model.

5.2.3 Local Edge Detectors and Orientation-Selective Units

Early visual systems possess local edge detectors and orientation-selective units [52, 4]. While convolutional neural networks have been successfully trained to detect boundaries via supervised learning [63], their initial layers have not shown proficiency in edge detection [47]. Does the even coding IPU model resemble biological systems more closely? To answer this, we trained an IPU on 4×4 grayscale image patches and applied it to images with a stride of 1 pixel, generating feature maps for each output node. The model comprises a MLP with 64 outputs and an intermediary layer with 100 nodes. Fig. 4 illustrates the feature maps of 4 output nodes of the IPU. It also shows edges generated by the Canny edge detector as comparison. Interestingly, with this simple network architecture, the even coding IPU model demonstrated a remarkable capability in edge detection.

Furthermore, Fig. 5 shows the feature maps of 5 output nodes for a sample bike image. Spokes of different orientations activate different nodes, indicating that these output nodes of the even coding IPU model have varying orientation preferences, similar to orientation-selective units found in biological systems.

5.2.4 Luminance and Color

Previous studies on image patch representation have often focused on contrast while ignoring the average luminance of image patches. For instance, in ICA or the sparse coding method, average luminance information is lost after preprocessing steps. However, without taking luminance into account, we cannot build a complete model of image patches and fully understand the early visual system. Firstly, a statistically significant portion of image patches, such as those extracted from the

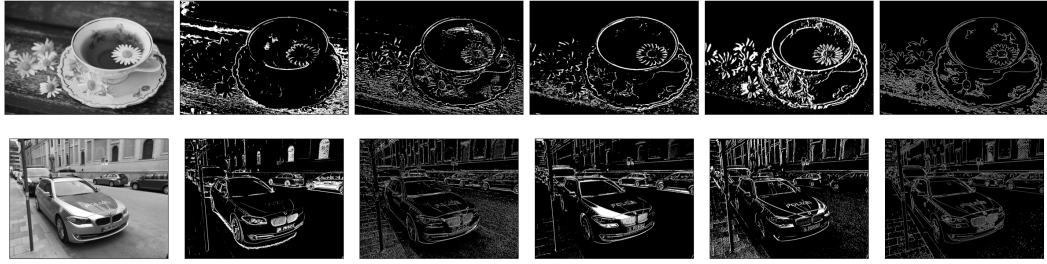


Figure 4: Feature maps of nodes resembling local edge detectors. The first column presents the grayscale test images. Each subsequent column, except the last one, displays the feature maps corresponding to the same output node for the test images. The last column shows edges generated by the multi-stage Canny edge detector for comparison.

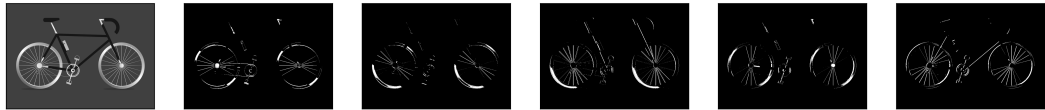


Figure 5: Test image and feature maps of 5 orientation-selective nodes.

sky or skin, exhibit little contrast and are primarily defined by their luminance (as well as color for color images). Secondly, research has shown that local luminance and contrast are nearly statistically independent in natural images [22, 59]. Thirdly, experimental results demonstrate that luminance is encoded by the visual system [80, 82, 65] and interacts with other properties of the early visual system [53, 103, 67, 77, 99].

When training even coding IPU model, we refrain from using any image preprocessing techniques, such as whitening, to preserve luminance information. As a result, the image IPU must learn to encode varying luminance levels in addition to contrast, using a binary population code. To explore the IPU’s response to different homogeneous (approximately) luminance levels, we applied the same 5×5 color IPU to an input image with varying luminance on a linear grayscale, as shown in Fig. 6 (a). Approximately 60% of nodes are activated by the gray image. We plot the input image and feature maps of 5 nodes in Fig. 6 (a) (refer to Appendix H for more information). These results are consistent with experimental findings showing that neurons in the early visual system exhibit varying luminance tuning ranges [30, 8, 100, 62]. Additionally, they align with research indicating that light intensity is collectively encoded by neurons [67, 56].

We also tested the IPU model on an image featuring the visible spectrum of an equal-energy illuminant (E) on a linear scale [12] to understand its response to different homogeneous (approximately) colors. The responses from some color-activated nodes are displayed in Fig. 6 (b). We used the same nodes in the same order as in Fig. 6 (a). The first and second nodes are activated and inhibited, respectively, by a single, broad segment of colors on the spectrum. The third node shows more specific color selectivity and is only activated by a narrow segment of the color spectrum. Unlike the case with luminance, where nodes are activated only by a single segment on the grayscale, some nodes like the fourth and fifth are tuned to multiple segments of colors on the spectrum. These results are consistent with experimental findings showing that neurons have different chromatic tuning properties to encode color using a distributed code [101]. Overall, we found that approximately three-quarters of the output nodes could be activated by some portion of the spectrum input (see Appendix H). This aligns with experimental data suggesting that about 60% to 80% of V1 neurons are color-selective [39, 23, 94, 32]. More specifically, about one-quarter of nodes are only activated/inhibited by a single spectrum segment, and about half of the nodes are activated by multiple spectrum segments. No experimental evidence has yet been found to support or contradict these numbers.

The results also highlight that the same node can exhibit selectivity for different stimulus attributes such as luminance, color, edge, and orientation. This is consistent with the finding that neurons in the early visual system multiplex information about multiple stimulus properties [80, 23, 88, 20, 32].

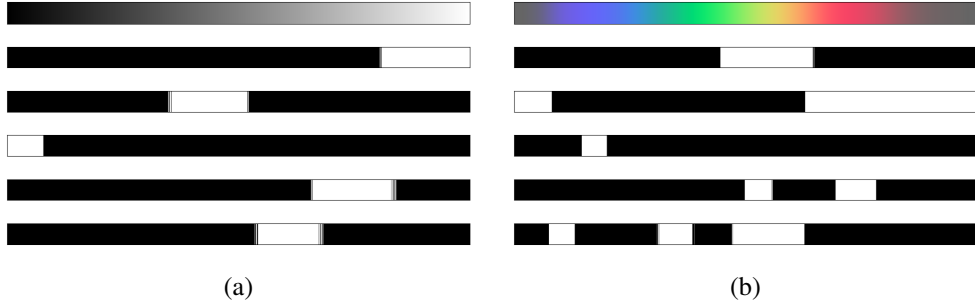


Figure 6: IPU’s response to varying gray luminance levels (a) and spectral colors (b). The first row displays the input images. Each subsequent row shows the response of the same node to both types of input.

6 Conclusion

In summary, we abstract the complex biological early visual system using four assumptions that serve as the foundation for all studies in this paper. We prove that maximizing information transmission and modeling the input probability distribution are not identical objectives. However, early-stage IPUs can pragmatically pursue both objectives using our even coding method.

According to even coding, we propose two types of unsupervised loss functions. The first, termed OBIS, explicitly enforces output statistics using 2D systems as examples, but it also applies to higher dimensions. The second achieves even coding implicitly by making response vectors repel each other, thereby resulting in a binary representation, as demonstrated in the image patch cases. Both types of loss functions require only local knowledge at the outputs, providing a more biologically plausible model for neural implementation compared to works that require non-local information for both input and output.

We confirm that the nonlinear even coding IPU produces statistically independent responses. The trained image patch IPU model also exhibits remarkable similarities to early visual systems, including multiplexing, nonlinear population code, binary signals, and uncorrelated outputs [19]. Additionally, it features local edge-detecting and orientation-selective units, as well as nodes with different luminance and chromatic tuning properties. Moreover, when compared to a deep learning model, the efficiency of our image patch IPU model outperforms it by a significant margin.

There are several intriguing directions for future research:

1. Although the loss function for image patches yields results closely resemble those of biological systems, its use of binary code aligns it more with temporal coding rather than rate coding. For rate coding, the OBIS loss function is more compatible. Thus, is there another way to resolve the two issues outlined at the beginning of Section 5 without introducing a new loss function?
2. For simplicity, we focus on the noiseless case in this study. It would be interesting to investigate the effects of introducing noise to the model.
3. The IPU model accommodates a range of inputs, from simple one-pixel instances to complex color image patches. Could the model’s application extend beyond the early stages of visual information processing?
4. The even coding model could be readily extended to handle video data by adding a time dimension. A detailed comparison with early visual systems would be of great value.
5. The even coding model also has the potential to adapt to binocular vision data by incorporating an additional input dimension of size two. Investigating whether the model can detect binocular disparity or even construct a 3D model of the world would be fascinating.
6. A vital avenue for future research involves understanding how biological systems might implement even coding. Could mechanisms such as lateral inhibition and homeostatic plasticity play roles?

7. While this paper primarily addresses visual information, the versatility of the even coding model suggests its applicability to modeling other multivariate probability distributions.
8. From an application standpoint, the even coding model holds potential in various areas including local edge detection, image and video compression, denoising, retrieval, texture classification, and multispectral/hyperspectral image processing.

Acknowledgments and Disclosure of Funding

I am grateful for the interdisciplinary doctoral fellowship (IDK-NBT) provided by the Center for NanoScience (CeNS) of LMU and the Elite Network of Bavaria, which funded my attendance at NeurIPS 2011, where I became inspired to work on this problem. I would like to thank Jonathan Shock, Dean Rance, Jonathan Pillow and E.J. Chichilnisky for their valuable comments and feedback on the manuscript of this paper. I thank the anonymous reviewers of a previous version of this manuscript for their constructive comments, which greatly improved the presentation. This research was conducted independently by the author, without the use of any institutional resources or the endorsement of any institution.

References

- [1] Ehsaneddin Asgari and Mohammad RK Mofrad. Continuous distributed representation of biological sequences for deep proteomics and genomics. *PloS one*, 10(11):e0141287, 2015.
- [2] Joseph J. Atick. Could information theory provide an ecological theory of sensory processing? *Network: Computation in neural systems*, 3(2):213–251, 1992.
- [3] Fred Attneave. Some informational aspects of visual perception. *Psychological review*, 61(3):183, 1954.
- [4] Tom Baden, Philipp Berens, Katrin Franke, Miroslav Román Rosón, Matthias Bethge, and Thomas Euler. The functional diversity of retinal ganglion cells in the mouse. *Nature*, 529(7586):345–350, 2016.
- [5] Wyeth Bair and Christof Koch. Temporal precision of spike trains in extrastriate cortex of the behaving macaque monkey. *Neural computation*, 8(6):1185–1202, 1996.
- [6] Pierre F Baldi and Kurt Hornik. Learning in linear neural networks: A survey. *IEEE Transactions on neural networks*, 6(4):837–858, 1995.
- [7] Horace B Barlow et al. Possible principles underlying the transformation of sensory messages. *Sensory communication*, 1(01):217–233, 1961.
- [8] RB Barlow, DM Snodderly, and HA Swadlow. Intensity coding in primate visual system. *Experimental Brain Research*, 31:163–177, 1978.
- [9] Anthony J Bell and Terrence J Sejnowski. The “independent components” of natural scenes are edge filters. *Vision research*, 37(23):3327–3338, 1997.
- [10] Michael J. Berry, David K. Warland, and Markus Meister. The structure and precision of retinal spike trains. *Proceedings of the National Academy of Sciences of the United States of America*, 94(10):5411–5416, may 1997.
- [11] Michael Beyeler, Emily L. Rounds, Kristofor D. Carlson, Nikil Dutt, and Jeffrey L. Krichmar. Neural correlates of sparse coding and dimensionality reduction. *PLOS Computational Biology*, 15(6):e1006908, jun 2019.
- [12] Bhutajata. Visible spectrum on a linear scale, 2017.
- [13] Jane Bromley, Isabelle Guyon, Yann LeCun, Eduard Säckinger, and Roopak Shah. Signature verification using a "siamese" time delay neural network. *Advances in neural information processing systems*, 6, 1993.

- [14] Daniel A. Butts, Chong Weng, Jianzhong Jin, Chun I. Yeh, Nicholas A. Lesica, Jose Manuel Alonso, and Garrett B. Stanley. Temporal precision in the neural code and the timescales of natural vision. *Nature* 2007 449:7158, 449(7158):92–95, sep 2007.
- [15] Matteo Carandini, Jonathan B. Demb, Valerio Mante, David J. Tolhurst, Yang Dan, Bruno A. Olshausen, Jack L. Gallant, and Nicole C. Rust. Do We Know What the Early Visual System Does? *Journal of Neuroscience*, 25(46):10577–10597, nov 2005.
- [16] Ting Chen, Simon Kornblith, Mohammad Norouzi, and Geoffrey Hinton. A simple framework for contrastive learning of visual representations. In *International conference on machine learning*, pages 1597–1607. PMLR, 2020.
- [17] Peter Dayan and Laurence F Abbott. *Theoretical neuroscience: computational and mathematical modeling of neural systems*. MIT press, 2005.
- [18] Jia Deng, Wei Dong, Richard Socher, Li-Jia Li, Kai Li, and Li Fei-Fei. Imagenet: A large-scale hierarchical image database. In *2009 IEEE conference on computer vision and pattern recognition*, pages 248–255. Ieee, 2009.
- [19] Alexander S Ecker, Philipp Berens, Georgios A Keliris, Matthias Bethge, Nikos K Logothetis, and Andreas S Tolias. Decorrelated neuronal firing in cortical microcircuits. *science*, 327(5965):584–587, 2010.
- [20] Stephen A Engel. Adaptation of oriented and unoriented color-selective neurons in human visual areas. *Neuron*, 45(4):613–623, 2005.
- [21] David J. Field. What Is the Goal of Sensory Coding? *Neural Computation*, 6(4):559–601, jul 1994.
- [22] Robert A Frazor and Wilson S Geisler. Local luminance and contrast in natural images. *Vision research*, 46(10):1585–1598, 2006.
- [23] Howard S Friedman, Hong Zhou, and Rüdiger von der Heydt. The coding of uniform colour figures in monkey visual cortex. *The Journal of physiology*, 548(2):593–613, 2003.
- [24] Deep Ganguli and Eero P Simoncelli. Efficient sensory encoding and bayesian inference with heterogeneous neural populations. *Neural computation*, 26(10):2103–2134, 2014.
- [25] Stuart Geman and Donald Geman. Stochastic relaxation, gibbs distributions, and the bayesian restoration of images. *IEEE Transactions on pattern analysis and machine intelligence*, (6):721–741, 1984.
- [26] Wulfram Gerstner, Werner M Kistler, Richard Naud, and Liam Paninski. *Neuronal dynamics: From single neurons to networks and models of cognition*. Cambridge University Press, 2014.
- [27] Ian Goodfellow, Jean Pouget-Abadie, Mehdi Mirza, Bing Xu, David Warde-Farley, Sherjil Ozair, Aaron Courville, and Yoshua Bengio. Generative adversarial nets. *Advances in neural information processing systems*, 27, 2014.
- [28] Cheng Guo and Felix Berkhahn. Entity embeddings of categorical variables. *arXiv preprint arXiv:1604.06737*, 2016.
- [29] Torkel Hafting, Marianne Fyhn, Sturla Molden, May Britt Moser, and Edvard I. Moser. Microstructure of a spatial map in the entorhinal cortex. *Nature* 2005 436:7052, 436(7052):801–806, jun 2005.
- [30] Robert W Hammon and Robert P Scobey. The luminance and response range of monkey retinal ganglion cells to white light. *Vision Research*, 22(2):271–277, 1982.
- [31] Peter JB Hancock, Roland J Baddeley, and Leslie S Smith. The principal components of natural images. *Network: computation in neural systems*, 3(1):61, 1992.
- [32] Charles A Hass and Gregory D Horwitz. V1 mechanisms underlying chromatic contrast detection. *Journal of Neurophysiology*, 109(10):2483–2494, 2013.

- [33] Demis Hassabis, Dharshan Kumaran, Christopher Summerfield, and Matthew Botvinick. Neuroscience-Inspired Artificial Intelligence. *Neuron*, 95(2):245–258, 2017.
- [34] G. E. Hinton and R. R. Salakhutdinov. Reducing the Dimensionality of Data with Neural Networks. *Science*, 313(5786):504–507, 2006.
- [35] Geoffrey E Hinton. Training products of experts by minimizing contrastive divergence. *Neural computation*, 14(8):1771–1800, 2002.
- [36] Geoffrey E Hinton and Ruslan R Salakhutdinov. Reducing the dimensionality of data with neural networks. *science*, 313(5786):504–507, 2006.
- [37] Aapo Hyvärinen, Jarmo Hurri, and Patrick O Hoyer. *Natural image statistics: A probabilistic approach to early computational vision.*, volume 39. Springer Science & Business Media, 2009.
- [38] Eugene M Izhikevich. Which model to use for cortical spiking neurons? *IEEE transactions on neural networks*, 15(5):1063–1070, 2004.
- [39] Elizabeth N Johnson, Michael J Hawken, and Robert Shapley. The spatial transformation of color in the primary visual cortex of the macaque monkey. *Nature neuroscience*, 4(4):409–416, 2001.
- [40] Eric R Kandel, James H Schwartz, Thomas M Jessell, Steven Siegelbaum, A James Hudspeth, Sarah Mack, et al. *Principles of neural science*, volume 4. McGraw-hill New York, 2000.
- [41] Yan Karklin and Michael S. Lewicki. Emergence of complex cell properties by learning to generalize in natural scenes. *Nature*, 457(7225):83–86, jan 2009.
- [42] Yan Karklin and Eero Simoncelli. Efficient coding of natural images with a population of noisy linear-nonlinear neurons. *Advances in neural information processing systems*, 24, 2011.
- [43] Diederik P Kingma and Max Welling. Auto-encoding variational bayes. *arXiv preprint arXiv:1312.6114*, 2013.
- [44] David C Knill and Whitman Richards. *Perception as Bayesian inference*. Cambridge University Press, 1996.
- [45] Gregory Koch, Richard Zemel, Ruslan Salakhutdinov, et al. Siamese neural networks for one-shot image recognition. In *ICML deep learning workshop*, volume 2. Lille, 2015.
- [46] Simon Laughlin. A Simple Coding Procedure Enhances a Neuron’s Information Capacity. *Zeitschrift für Naturforschung C*, 36(9-10):910–912, oct 1981.
- [47] Minh Le and Subhadeep Kayal. Revisiting edge detection in convolutional neural networks. In *2021 International Joint Conference on Neural Networks (IJCNN)*, pages 1–9. IEEE, 2021.
- [48] Yann LeCun, Yoshua Bengio, and Geoffrey Hinton. Deep learning. *nature*, 521(7553):436–444, 2015.
- [49] Ann B Lee, Kim S Pedersen, and David Mumford. The Nonlinear Statistics of High-Contrast Patches in Natural Images. *International Journal of Computer Vision*, 54(5413):83–103, 2003.
- [50] Daniel Lee and Seung Sebastian. Learning the parts of objects by non-negative matrix factorization. *Nature*, 401:788, oct 1999.
- [51] Honglak Lee, Alexis Battle, Rajat Raina, and Andrew Ng. Efficient sparse coding algorithms. In B. Schölkopf, J. Platt, and T. Hoffman, editors, *Advances in Neural Information Processing Systems*, volume 19. MIT Press, 2006.
- [52] William R Levick. Receptive fields and trigger features of ganglion cells in the visual streak of the rabbit’s retina. *The Journal of physiology*, 188(3):285, 1967.
- [53] Xiaobing Li, Yao Chen, Reza Lashgari, Yulia Bereshpolova, Harvey A Swadlow, Barry B Lee, and Jose Manuel Alonso. Mixing of chromatic and luminance retinal signals in primate area v1. *Cerebral Cortex*, 25(7):1920–1937, 2015.

[54] Tsung-Yi Lin, Michael Maire, Serge Belongie, Lubomir Bourdev, Ross Girshick, James Hays, Pietro Perona, Deva Ramanan, C. Lawrence Zitnick, and Piotr Dollár. Microsoft coco: Common objects in context, 2014.

[55] Ralph Linsker. Self-organization in a perceptual network. *Computer*, 21(3):105–117, 1988.

[56] Andreas Liu, Elliott S Milner, Yi-Rong Peng, Hannah A Blume, Michael C Brown, Gregory S Bryman, Alan J Emanuel, Philippe Morquette, Nguyen-Minh Viet, Joshua R Sanes, et al. Encoding of environmental illumination by primate melanopsin neurons. *Science*, 379(6630):376–381, 2023.

[57] Wei Ji Ma, Jeffrey M. Beck, Peter E. Latham, and Alexandre Pouget. Bayesian inference with probabilistic population codes. *Nature Neuroscience* 2006 9:11, 9(11):1432–1438, oct 2006.

[58] Zachary F Mainen and Terrence J Sejnowski. Reliability of spike timing in neocortical neurons. *Science*, 268(5216):1503–1506, 1995.

[59] Valerio Mante, Robert A Frazor, Vincent Bonin, Wilson S Geisler, and Matteo Carandini. Independence of luminance and contrast in natural scenes and in the early visual system. *Nature neuroscience*, 8(12):1690–1697, 2005.

[60] Eve Marder and Adam L Taylor. Multiple models to capture the variability in biological neurons and networks. *Nature neuroscience*, 14(2):133–138, 2011.

[61] David Marr. *Vision: A Computational Investigation into the Human Representation and Processing of Visual Information*. The MIT Press, 07 2010.

[62] Richard T Marrocco. Possible neural basis of brightness magnitude estimations. *Brain Research*, 1975.

[63] David R Martin, Charless C Fowlkes, and Jitendra Malik. Learning to detect natural image boundaries using local brightness, color, and texture cues. *IEEE transactions on pattern analysis and machine intelligence*, 26(5):530–549, 2004.

[64] Richard H. Masland. The Neuronal Organization of the Retina, oct 2012.

[65] Reece Mazade, Jianzhong Jin, Hamed Rahimi-Nasrabadi, Sohrab Najafian, Carmen Pons, and Jose-Manuel Alonso. Cortical mechanisms of visual brightness. *Cell reports*, 40(13), 2022.

[66] Tomas Mikolov, Kai Chen, Greg Corrado, and Jeffrey Dean. Efficient estimation of word representations in vector space. *arXiv preprint arXiv:1301.3781*, 2013.

[67] Elliott Scott Milner and Michael Tri Hoang Do. A population representation of absolute light intensity in the mammalian retina. *Cell*, 171(4):865–876, 2017.

[68] Guido Montúfar, Razvan Pascanu, Kyunghyun Cho, and Yoshua Bengio. On the Number of Linear Regions of Deep Neural Networks. *Advances in Neural Information Processing Systems*, 4(January):2924–2932, feb 2014.

[69] Jean Pierre Nadal and Nestor Parga. Nonlinear neurons in the low-noise limit: a factorial code maximizes information transfer. http://dx.doi.org/10.1088/0954-898X_5_4_008, 5(4):565–581, 2009.

[70] Samuel Ocko, Jack Lindsey, Surya Ganguli, and Stephane Deny. The emergence of multiple retinal cell types through efficient coding of natural movies. *Advances in Neural Information Processing Systems*, 31, 2018.

[71] Benjamin Odermatt, Anton Nikolaev, and Leon Lagnado. Encoding of Luminance and Contrast by Linear and Nonlinear Synapses in the Retina. *Neuron*, 73:758–773, 2012.

[72] Bruno A Olshausen. sparse codes and spikes. *Probabilistic models of the brain*, page 257, 2002.

[73] Bruno A. Olshausen and David J. Field. Emergence of simple-cell receptive field properties by learning a sparse code for natural images. *Nature*, 381(6583):607–609, oct 1996.

- [74] Bruno A Olshausen and David J Field. Sparse coding with an overcomplete basis set: A strategy employed by v1? *Vision research*, 37(23):3311–3325, 1997.
- [75] Bruno A Olshausen and David J Field. Sparse coding of sensory inputs. *Current opinion in neurobiology*, 14(4):481–487, 2004.
- [76] Simon Osindero and Geoffrey Hinton. Modeling image patches with a directed hierarchy of Markov random fields. In *Advances in Neural Information Processing Systems 20 (NIPS'07)*, pages 1121–1128. 2008.
- [77] Hamed Rahimi-Nasrabadi, Jianzhong Jin, Reece Mazade, Carmen Pons, Sohrab Najafian, and Jose-Manuel Alonso. Image luminance changes contrast sensitivity in visual cortex. *Cell reports*, 34(5), 2021.
- [78] Marc Aurelio Ranzato and Geoffrey E Hinton. Factored 3-Way Restricted Boltzmann Machines For Modeling Natural Images. In *AISTATS '10*, volume 9, pages 621–628, 2010.
- [79] Marc’Aurelio Ranzato, Christopher Poultney, Sumit Chopra, and Yann Cun. Efficient learning of sparse representations with an energy-based model. *Advances in neural information processing systems*, 19, 2006.
- [80] Andrew F. Rossi, Cynthia D. Rittenhouse, and Michael A. Paradiso. The representation of brightness in primary visual cortex. *Science*, 273:1104–1107, 8 1996.
- [81] Stefan Roth and Michael J Black. Fields of experts: A framework for learning image priors. In *2005 IEEE Computer Society Conference on Computer Vision and Pattern Recognition (CVPR'05)*, volume 2, pages 860–867. IEEE, 2005.
- [82] Douglas A Ruff, David H Brainard, and Marlene R Cohen. Neuronal population mechanisms of lightness perception. *Journal of Neurophysiology*, 120(5):2296–2310, 2018.
- [83] Joshua R. Sanes and S. Lawrence Zipursky. Design Principles of Insect and Vertebrate Visual Systems, 2010.
- [84] Steffen Schneider, Alexei Baevski, Ronan Collobert, and Michael Auli. wav2vec: Unsupervised pre-training for speech recognition. *arXiv preprint arXiv:1904.05862*, 2019.
- [85] Florian Schroff, Dmitry Kalenichenko, and James Philbin. Facenet: A unified embedding for face recognition and clustering. In *Proceedings of the IEEE conference on computer vision and pattern recognition*, pages 815–823, 2015.
- [86] Odelia Schwartz and Eero P Simoncelli. Natural signal statistics and sensory gain control. *Nature neuroscience*, 4(8):819–825, 2001.
- [87] C. E. Shannon. A Mathematical Theory of Communication. *Bell System Technical Journal*, 27(3):379–423, 1948.
- [88] Robert Shapley and Michael J Hawken. Color in the cortex: single-and double-opponent cells. *Vision research*, 51(7):701–717, 2011.
- [89] Eero P Simoncelli. Vision and the statistics of the visual environment. *Current Opinion in Neurobiology*, 13(2):144–149, 2003.
- [90] Eero P. Simoncelli. Optimal Estimation in Sensory Systems. In *The New Cognitive Neurosciences*. MIT Press, 2009.
- [91] Eero P Simoncelli and Bruno A Olshausen. Natural image statistics and neural representation. *Annual review of neuroscience*, 24(1):1193–1216, 2001.
- [92] Karen Simonyan and Andrew Zisserman. Very deep convolutional networks for large-scale image recognition. *arXiv preprint arXiv:1409.1556*, 2014.
- [93] Alan A Stocker and Eero P Simoncelli. Noise characteristics and prior expectations in human visual speed perception. *Nature neuroscience*, 9(4):578–585, 2006.

[94] Lisa G Thorell, Russell L de Valois, and Duane G Albrecht. Spatial mapping of monkey vi cells with pure color and luminance stimuli. *Vision research*, 24(7):751–769, 1984.

[95] Michael E Tipping and Christopher M Bishop. Probabilistic principal component analysis. *Journal of the Royal Statistical Society Series B: Statistical Methodology*, 61(3):611–622, 1999.

[96] J Hans van Hateren and Dan L Ruderman. Independent component analysis of natural image sequences yields spatio-temporal filters similar to simple cells in primary visual cortex. *Proceedings of the Royal Society of London. Series B: Biological Sciences*, 265(1412):2315–2320, 1998.

[97] JH van Hateren. A theory of maximizing sensory information. *Biol. Cybern*, 68:23–29, 1992.

[98] Benjamin T Vincent and Roland J Baddeley. Synaptic energy efficiency in retinal processing. *Vision research*, 43(11):1285–1292, 2003.

[99] Louis N Vinke and Sam Ling. Luminance potentiates human visuocortical responses. *Journal of Neurophysiology*, 123(2):473–483, 2020.

[100] Béla Völgyi, Michael R Deans, David L Paul, and Stewart A Bloomfield. Convergence and segregation of the multiple rod pathways in mammalian retina. *Journal of Neuroscience*, 24(49):11182–11192, 2004.

[101] Thomas Wachtler, Terrence J Sejnowski, and Thomas D Albright. Representation of color stimuli in awake macaque primary visual cortex. *Neuron*, 37(4):681–691, 2003.

[102] Xue Xin Wei and Alan A. Stocker. A Bayesian observer model constrained by efficient coding can explain 'anti-Bayesian' percepts. *Nature Neuroscience* 2015 18:10, 18(10):1509–1517, sep 2015.

[103] Sophia Wienbar and Gregory W Schwartz. The dynamic receptive fields of retinal ganglion cells. *Progress in retinal and eye research*, 67:102–117, 2018.

[104] Thomas E Yerxa, Eric Kee, Michael R DeWeese, and Emily A Cooper. Efficient sensory coding of multidimensional stimuli. *PLoS computational biology*, 16(9):e1008146, 2020.

[105] Daniel Zoran and Yair Weiss. From learning models of natural image patches to whole image restoration. In *2011 international conference on computer vision*, pages 479–486. IEEE, 2011.

A Proof: Maximizing Transmission Rate is Equivalent to Maximizing H_Q

The rate of transmission is defined according to Shannon's information theory [87] as:

$$R = H_Q - H(y|x), \quad (17)$$

where $H(y|x)$ is the conditional entropy of y given x . This can be defined as:

$$H(y|x) = - \sum_{i,j} p(x_i, y_j) \log p(y_j|x_i) \quad (18)$$

$$= - \sum_{i,j} p(x_i) p(y_j|x_i) \log p(y_j|x_i) \quad (19)$$

$$= - \sum_i \left[p(x_i) \sum_j p(y_j|x_i) \log p(y_j|x_i) \right], \quad (20)$$

where $p(x_i, y_j)$ is the joint probability of x and y and $p(y_j|x_i)$ is the conditional probability - that is, the probability of the output value being y_j given that we know the input is x_i .

Now, for a deterministic model where each input x_i maps to one and only one output y_j , we can have $p(y_j|x_i)$ being 1 for some j and 0 for the others. As a result, the expression $p(y_j|x_i) \log p(y_j|x_i)$ is always 0, whether $p(y_j|x_i)$ is 0 or 1. Therefore, we have $H(y|x) = 0$. Consequently, the rate of transmission R simplifies to $R = H_Q$. Hence, maximizing the rate of transmission is equivalent to maximizing H_Q .

B Proof: Cross-Entropy H_{pq} is Equivalent to H_q

Under the condition Eq. (3) and Eq. (4) specified in the main text, we can rewrite the cross-entropy H_{pq} as:

$$H_{pq} = - \sum_x p(x) \log q(x) \quad (21)$$

$$= - \sum_{j=1}^N \sum_{x \in G_j} p(x) \log q(x) \quad (22)$$

$$= - \sum_{j=1}^N \sum_{x \in G_j} p(x) \log \frac{Q(y_j)}{n_j} \quad (23)$$

$$= - \sum_{j=1}^N \log \frac{Q(y_j)}{n_j} \sum_{x \in G_j} p(x) \quad (24)$$

$$= - \sum_{j=1}^N Q(y_j) \log \frac{Q(y_j)}{n_j}. \quad (25)$$

Similarly, we can express H_q as:

$$H_q = - \sum_x q(x) \log q(x) \quad (26)$$

$$= - \sum_{j=1}^N \sum_{x \in G_j} q(x) \log q(x) \quad (27)$$

$$= - \sum_{j=1}^N \sum_{x \in G_j} q_j \log q_j \quad (28)$$

$$= - \sum_{j=1}^N Q(y_j) \log \frac{Q(y_j)}{n_j}. \quad (29)$$

Comparing the two results, we have

$$H_{pq} = H_q. \quad (30)$$

C Proof of Necessary and Sufficient Conditions for Orthogonality of Bases in Two-Pixel Case

We want the outputs of the two MLPs to be independent, meaning we cannot predict the state of the second MLP's output given the first one:

$$Q(y_2|y_1) = Q(y_2). \quad (31)$$

Additionally, we want each MLP to partition the input space evenly. This is represented as:

$$Q(y_1) = \frac{1}{N_1}, Q(y_2) = \frac{1}{N_2}, \quad (32)$$

where N_1 and N_2 represent the number of output nodes of the two MLPs. Eq. (31) and Eq. (32) leads to

$$Q(y_1, y_2) = \frac{1}{N_1 N_2}. \quad (33)$$

Conversely, from Eq. (33), we can derive Eq. (31) and Eq. (32), indicating they are equivalent. Therefore, we conclude that the bases are orthogonal if and only if Eq. (33) is satisfied.

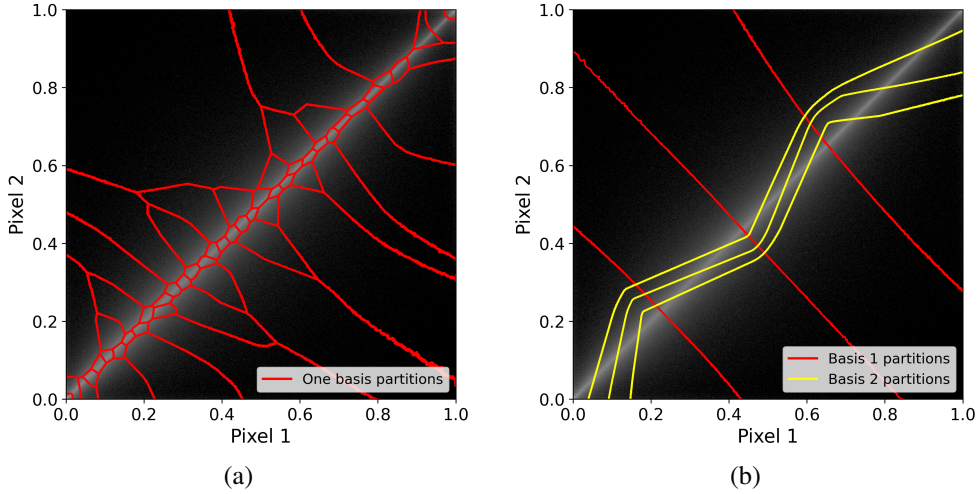


Figure 7: Additional results complementing Fig. 1 in the main text. (a) One basis with 64 independent states. The 2D structure of the even partition is complex, reflecting the high expressiveness of the MLP in modeling the probability space. (b) Two orthogonal bases, each with 4 independent states. The second MLP has learned to employ a zigzag partitioning structure, effectively dividing the total intensity into more sections. This suggests that the model may be compensating for the perceived insufficiency of the first MLP in partitioning the total intensity with only 4 states.

D Experimental Details and Supplementary Results for the Two-Pixel Case

To ensure that the multi-layer perceptron (MLP) models were versatile enough to approximate complex functions [68], we employed relatively large MLPs with two hidden layers of 200 and 100 nodes, respectively. The Rectified Linear Unit (ReLU) is used as the activation function.

For training data, we randomly sampled 10 million pairs of horizontally neighboring pixels from the COCO dataset [54]. The models were trained for 20 epochs using Adam optimizer with a learning rate of 0.001. In the experiments involving two MLPs, we used MLPs of the same size and followed the same training procedure as in the single MLP case. For the factor balancing the two terms in the loss function in Eq. (12) and Eq. (14) in the main text, we use $k = 2/3$ in all experiments.

The partitions were visualized using the tricontour function from matplotlib, which generates contour plots of unstructured triangular grids. The two pixel values were input as the x and y coordinates, while the outputs of the MLPs were used as the z-values.

In addition to Fig. 1 in the main text, some interesting results are shown in Fig. 7.

E Experimental Details for the Image Patches Case

Two models were discussed in the main text of our study: a model trained on 5×5 color image patches (the color model), and another trained on 4×4 grayscale image patches (the grayscale model).

Grayscale Model: Our training data consisted of roughly 100,000 images from the unlabeled section of the COCO 2017 image dataset, converted to grayscale. In each training batch, we randomly selected 1,000 images and extracted 1,000 random image patches from each image, leading to a total of 1 million image patches per batch. From this batch, a mini-batch of 500 patches was randomly chosen to calculate the loss function. To ensure numerical stability, a small value $\epsilon = 10^{-38}$ was added when computing the distances between samples. We used the Adam optimizer with a learning rate of 1e-3, and the model was trained for a single epoch. The sparsity regularization parameter was set to $\alpha = 0.05$.

Color Model: Training data for the color model were image patches extracted from 1.2 million images in the training portion of ImageNet. Each training batch comprised 500 randomly chosen

images, with 100 random image patches extracted from each image. From each batch, a mini-batch of 500 patches was sequentially selected (i.e., patches within each batch were not shuffled) to compute the loss function. To augment the dataset, we randomly flipped images horizontally with a probability of 0.5. We adopted the node-wise repel form of the loss function to ensure numerical stability (comparable results were achieved with the method used in the grayscale model). The model was trained for 10 epochs using the AdamW optimizer, with a learning rate of 2e-4 for the first 5 epochs, and 1e-4 for the remaining epochs. The sparsity regularization parameter was set to $\alpha = \frac{6}{96} = 0.0625$.

F Statistical Analysis of Even Code Representation

In this section, we conduct further statistical analyses on the even code representation using the grayscale model described in Appendix E. Fig. 8 (a) illustrates the proportion of samples activating each unique binary representation. At the most granular level, the distribution is highly uneven, reflecting the image similarity statistics learned by the model, as anticipated. Fig. 8 (b) shows the proportion of samples activating a certain number of output nodes, with the majority activating around 14 out of the 64 total output nodes.

To confirm that samples also have a relatively even distribution at middle scales, We select 30 random occupied positions in the binary representation space and count the total number of samples within varying distances to each. If the distribution is relatively even, the 30 curves should be close to each other (within the same order of magnitude) and exhibit similar shapes. The result is shown in Fig. 8 (c). Most curves are close even at the smallest scale, and they become closer as the scale increases In Fig. 8 (d) we plot the occupancy rate of positions in the binary representation space at different distances to 30 random occupied positions. The occupancy rate is calculated as the total number of samples at a distance d to a random occupied position, divided by the number of all possible sites in the binary space with a distance d to the same position, which is the combination number $\binom{64}{d}$. A similar decaying trend is observed for all 30 random sites, except at a small scale or at a large d , where the boundary of the subspace is reached.

G Decoding Even Code

To intuitively understand how well the binary representation preserves information, we can decode the binary representations and compare them to the original image patches. The encoder model and its training is the same with the grayscale model described in Appendix E except here we use color images and $\alpha = 0.03$.

To train the decoder, 10 million random image patches are fed into the encoder to generate corresponding representations. Since the mapping is many-to-one, we average all image patches with the same binary representation as the training target and use the binary vector as the feature. This results in approximately half a million feature-target pairs for training the decoder. We use an MLP with the same size as the encoder to construct the decoder, which is trained with a batch size of 128 for 100 epochs, using the Adam optimizer and a learning rate of 0.001.

Once the decoder is trained, we first use the encoder to encode every non-overlapping image patch of an image. Then, the decoder is used to convert the binary representations back into image patches, which are then tilted together to get the decoded image. Fig. 9 shows an example of original and decoded images. While the even code method does not explicitly optimize for image reconstruction performance in the loss function, unlike many previous image patch modeling methods [50, 51, 76, 78, 73], it is noteworthy that the binary representation preserves critical information such as luminance, color, and boundaries effectively. This retention of key details ensures the accurate comprehension of the image in subsequent processing stages.

H Complete output response to different gray levels and colors

Fig. 10 and Fig. 11 display the responses of all 96 outputs from the 5×5 color IPU model to linear grayscale and spectral color inputs, as shown in Fig. 6 in the main text. Both input images have dimensions of 1920 by 90 pixels. The IPU processes the input images with a stride of 1 pixel, producing feature maps for each output node.

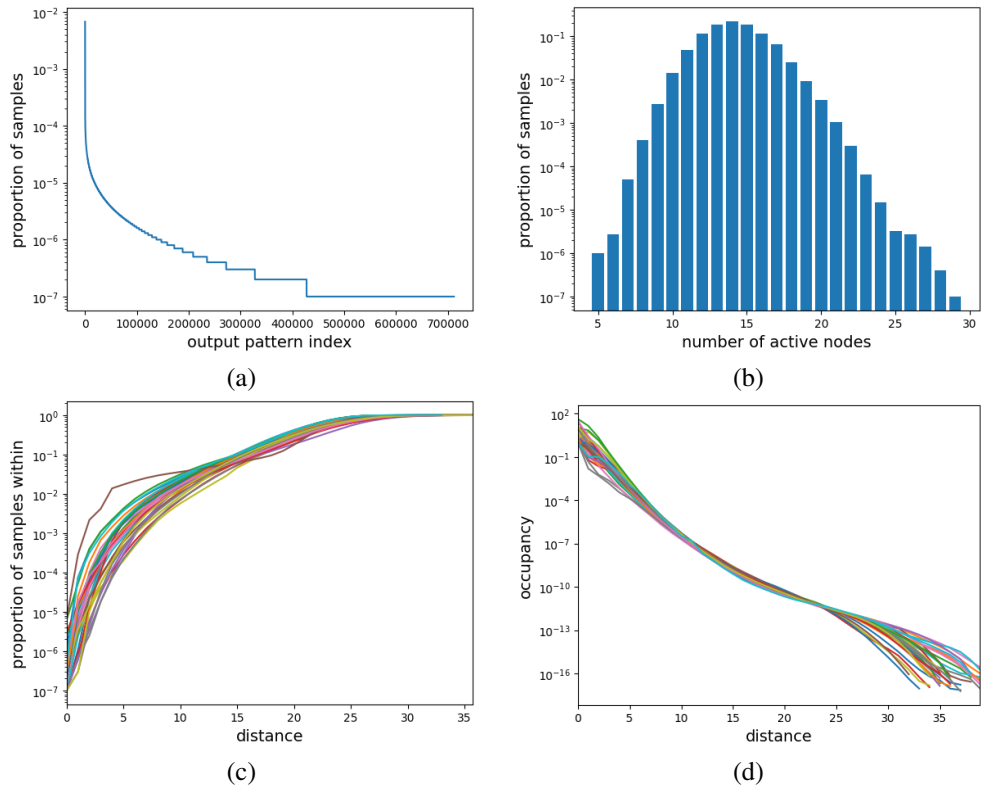


Figure 8: Statistical analysis of the learned representation using the loss function Eq. (16) defined in the main text. (a) Proportion of image patch samples activating each unique representation pattern. (b) Proportion of image patch samples with representation having different numbers of active nodes. (c) Proportion of image patch samples within varying distances to 30 random positions in the binary representation space. (d) Occupancy rate at different distances to 30 random positions in the binary representation space.



Figure 9: Demonstration of decoding the binary representation. (a) The original image. (b) The image reconstructed from decoded image patches, which are titled together. Despite the lack of explicit optimization for image reconstruction, key details such as luminance, color, and boundaries are preserved effectively.

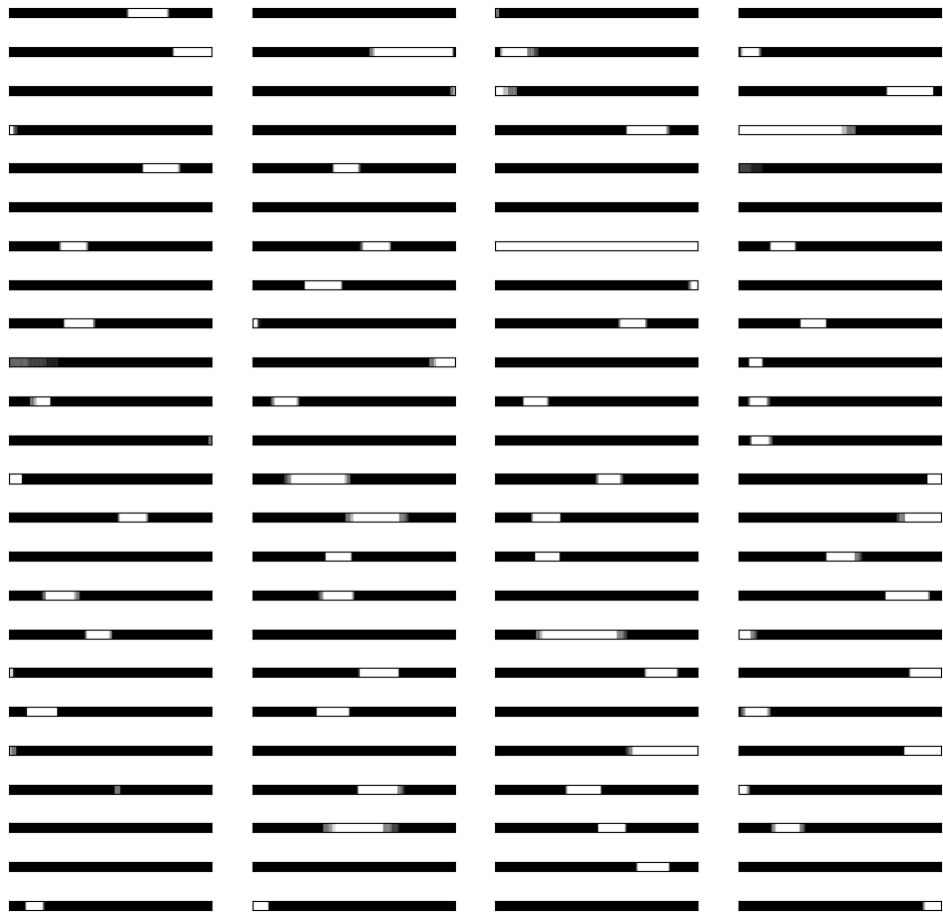


Figure 10: Response of all 96 outputs from the 5×5 color IPU model to the linear grayscale input.

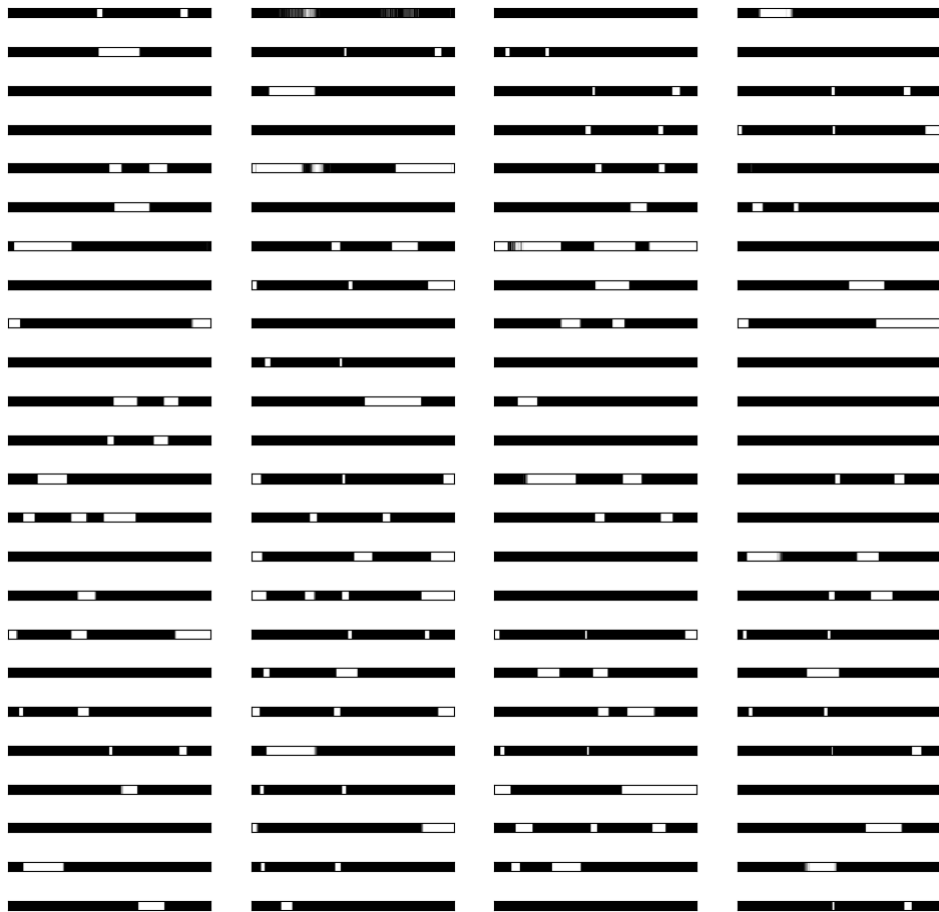


Figure 11: Response of all 96 outputs from the 5×5 color IPU model to the spectral color input.